JOURNAL OF VIROLOGY, June 2009, p. 5466–5476 Vol. 83, No. 11
0022-538X/09/$08.00+0 doi:10.1128/JVI.02670-08

Varicella-Zoster Virus Infection Induces Autophagy in both Cultured Cells and Human Skin Vesicles[▽]

Marie-Noëlle Takahashi,[1] Wallen Jackson,[3] Donna T. Laird,[1] Timothy D. Culp,[2] Charles Grose,[3] John I. Haynes II,[1]* and Luca Benetti[1]*

Global Vaccines Technology and Engineering-Bioanalytics, Merck Manufacturing Division,[1] and Bioprocess Analytical and Formulation Sciences, Merck Research Laboratories,[2] Merck & Co., Inc., West Point, Pennsylvania 19486, and University of Iowa College of Medicine, Iowa City, Iowa 52242[3]

Received 29 December 2008/Accepted 12 March 2009

When grown in cultured cells, varicella-zoster virus (VZV) forms many aberrant light particles and produces low titers. Various studies have explored the reasons for such a phenotype and have pointed to impaired expression of specific late genes and at lysosomal targeting of egressing virions as possible causes. In the studies presented here, we report that the autophagic degradation pathway was induced at late time points after VZV infection of cultured cells, as documented by immunoblot analysis of the cellular proteins LC3B and p62/SQSTM1, along with electron microscopy analysis, which demonstrated the presence of both early autophagosomes and late autophagic compartments. Autophagy was induced in infected cells even in the presence of phosphonoacetic acid, an inhibitor of viral late gene expression, thus suggesting that accumulation of immediate-early and early viral gene products might be the major stimulus for its induction. We also showed that the autophagic response was not dependent on a specific cell substrate, virus strain, or type of inoculum. Finally, using immunofluorescence imaging, we demonstrated autophagosome-specific staining in human zoster vesicles but not in normal skin. Thus, our results document that this innate immune response pathway is a component of the VZV infectious cycle in both cultured cells and the human skin vesicle, the final site of virion formation in the infected human host.

Varicella-zoster virus (VZV) is a neurotropic alphaherpesvirus that infects humans. VZV causes varicella (known by the common name chicken pox) during primary infection and herpes zoster (shingles) upon reactivation from latency (7). VZV is a ubiquitous pathogen, and incidence of varicella per year had until recently been virtually overlapping with the birth rate. However, this incidence has decreased dramatically since the introduction of a live attenuated varicella vaccine (16, 18, 43, 44).

Although infectious VZV particles are very abundant in skin vesicles during natural infection, in cultured cells the virus grows to very low titers and remains extremely cell associated, with noninfectious light particles (L particles) constituting the majority of particles on the surface of infected cells (4). A recent paper from Storlie et al. (42), reporting a delayed accumulation of the late VZV protein glycoprotein C (gC), suggested that an impairment in the expression of specific viral genes during infection of cultured cells could contribute to such low titers (4). An alternative and not mutually exclusive explanation for the low yields of VZV comes from a separate set of reports, which showed that egressing VZV particles acquire the final envelope at the level of the trans-Golgi network (13) and are then detectable both on the cell surface and within large cytoplasmic vacuoles. It has been reported that the egressing virions are degraded in such vacuoles by lysosomal acid hydrolases (13) and that the cation-independent mannose-6-phosphate receptor (MPR^{ci}) plays a role in such vacuolar accumulation (6).

Various publications have also recently begun to address the relationship between virus infection and macroautophagy (hereafter referred to as autophagy), a degradation pathway in which bulk amounts of cytoplasm are sequestered by double-membrane vesicles (12, 39). Such vesicles, termed autophagosomes, ultimately fuse with lysosomes, resulting in formation of autophagic compartments, in which the engulfed cytoplasmic material is degraded (39). At the molecular level, a number of evolutionarily conserved proteins, called *au*tophag*y*-related (Atg) proteins, are necessary for autophagosome formation (23). Autophagy assays in mammalian cells frequently involve analysis of the LC3B isoform of microtubule-associated protein 1 light chain 3 (LC3), an ortholog of yeast Atg8 (21, 22, 33). LC3B is present as a cytosolic form named LC3B-I, which during autophagy is conjugated to phosphatidylethanolamine (PE). The resulting form, LC3B-II, is associated with autophagosomal membranes and is essential for autophagosome formation (46). Formation of autophagosomes can be detected by immunofluorescence analysis, as the staining of LC3B-I is diffusely cytoplasmic, while the staining of LC3B-II is punctuate (21, 22). The two forms can also be separated by sodium dodecyl sulfate-polyacrylamide gel electrophoresis analysis, in which LC3B-I has a higher apparent M_r than LC3B-II (16,000 compared to 14,000). While the steady-state levels of LC3B-I and -II, as detected by immunoblotting, may vary among different cell lines or independent cultures of a cell line over long periods of time, the amount of LC3B-II among samples within

* Corresponding author. Mailing address: Merck & Co., Inc., WP17-101, 770 Sumneytown Pike, P.O. Box 4, West Point, PA 19486. Phone for John I. Haynes II: (215) 652-2671. Phone for Luca Benetti: (215) 652-9758. Fax: (215) 993-4851. E-mail for John I. Haynes II: john_haynes@merck.com. E-mail for Luca Benetti: luca_benetti@merck.com.

▽ Published ahead of print on 18 March 2009.

an individual experiment correlates with the number of autophagosomes (22, 45). A second commonly used method to detect autophagic flux involves monitoring the levels of polyubiquitin-binding protein p62/SQSTM1 (sequestosome 1). p62/SQSTM1 is a multifunctional protein that associates with protein aggregates, interacts with LC3B, and is selectively degraded by the autophagic-lysosome pathway (3, 24). Specifically, inhibition of autophagic degradation results in accumulation of p62/SQSTM1 (22, 24).

Autophagy was first reported as a response to starvation and has subsequently been associated with a variety of phenotypes, including neurodegenerative diseases, aging, cardiomyopathies, and cancer (8, 40). With regard to cell survival, it has been proposed that a physiological level of autophagy may contribute to cell homeostasis by allowing for turnover of long-lived proteins and disposal of damaged organelles and of aggregate-prone proteins; on the other hand, if induced beyond physiological ranges, autophagy may result in type II programmed cell death (35). Further, autophagy has also been reported to be part of the innate immune response against intracellular pathogens, including viruses (12, 28). For example, overexpression of the autophagy gene *Beclin1* blocked Sindbis virus-induced apoptosis of neurons (29), tobacco mosaic virus replicated to higher levels in plants in which expression of *beclin1* had been suppressed (30), and hepatitis C virus infection induced formation of autophagosomes in hepatocytes (1).

In the case of herpesviruses, different viruses appear to differentially modulate autophagy; in fact, herpes simplex virus type 1 (HSV-1), human cytomegalovirus, and murine gammaherpesvirus 68 have been shown to block completion of the autophagic pathway (2, 5, 26, 34), while Epstein-Barr virus latent membrane protein 1 has been reported to induce autophagy in Epstein-Barr virus-infected cells (27). No data investigating whether autophagy is involved in VZV infection have been reported so far. In the studies presented here we report that the autophagosome-associated form of LC3B accumulated late in VZV infection of cultured cells, concomitantly with degradation of p62/SQSTM1 and depletion of cytoplasmic material. VZV-induced autophagy markers were not affected by exposure to phosphonoacetic acid (PAA). We then extended our observations to show that induction of autophagy was not dependent on the cell type, virus strain, or type of inoculum (infected cells or cell free) used. Finally, we observed that autophagosomes were present in biopsies from human zoster vesicles but not in those from normal human skin. Thus, our data not only show that autophagy is a component of VZV infection in cultured cells but also report for the first time that autophagy is induced and may play an important role in a human tissue relevant to the pathogenesis of varicella and herpes zoster infections.

MATERIALS AND METHODS

Viruses and cells. The source of VZV used in most of the experiments reported was the Merck live attenuated varicella vaccine derived from the parent Oka strain (44) and hereafter referred to as vOka/Merck. Infected cell monolayers used as inocula were trypsinized when they showed >70% cytopathic effect (CPE), resuspended in freezing medium, and stored at −70°C. In selected experiments, the inoculum preparation originated from sonically disrupted infected MRC-5 cultures. Titers were determined by a plaque assay. Alternatively, a low-passage laboratory strain, VZV-32, was used where indicated. Both strains have been sequenced (14, 37, 47). MRC-5 cells, provided by the National Institute for Biological Standards and Control (NIBSC), or human melanoma cells, designated MeWo (17), were used in all experiments. Cells were maintained in either Dulbecco's modified Eagle's medium or Williams' minimal essential medium supplemented with 45 μg/ml neomycin, 2 mM L-glutamine, and either 10% bovine calf serum or 10% fetal bovine serum. At infection the medium was switched to Williams' minimal essential medium supplemented with 45 μg/ml neomycin, 2 mM L-glutamine, and either 10% or 2% bovine calf serum.

Antibodies and reagents. The primary antibodies used in these studies were as follows: mouse monoclonal antibody (MAb) anti-gC clone 233 (42), rabbit polyclonal monospecific anti-gC antibody R19 (41), a commercial mouse anti-gE MAb (Millipore, Billerica, MA), rabbit polyclonal anti-LC3B (Sigma, St. Louis, MO), anti-p62/SQSTM1 MAb (Santa Cruz Biotechnology Inc., Santa Cruz, CA), anti-β-actin MAb (Sigma), and anti-caspase 3 MAb (Cell Signaling Technology Inc., Danvers, MA). MAb anti-gE clone 3B3 was used in immunofluorescence experiments. The horseradish peroxidase-conjugated secondary antibodies were from Santa Cruz. PAA and the cathepsin inhibitor E64 were purchased from Sigma. The nuclear stain Draq5 was from Biostatus Limited (England).

Immunoblots. At the indicated time points, cells were scraped in their own medium, pelleted by low-speed centrifugation, and solubilized with radioimmunoprecipitation assay buffer from either Sigma (150 mM NaCl, 1.0% Igepal CA-630, 0.5% sodium deoxycholate, 0.1% sodium dodecyl sulfate, 50 mM Tris, pH 8.0) or Cell Signaling (20 mM Tris-HCl [pH 7.5], 150 mM NaCl, 1 mM Na_2EDTA, 1 mM EGTA, 1% NP-40, 1% sodium deoxycholate, 2.5 mM sodium pyrophosphate, 1 mM beta-glycerophosphate, 1 mM Na_3VO_4, 1 μg/ml leupeptin). The total protein concentration was measured with a bicinchoninic acid kit (Pierce, Rockford, IL) according to the manufacturer's instructions. Cell lysates, normalized to equal total protein concentrations, were diluted in lithium dodecyl sulfate–beta-mercaptoethanol (Invitrogen and Sigma) and heated at 75°C for 10 min. Samples were loaded on 10% or 4 to 12% NuPAGE gels (Invitrogen). Proteins were transferred to a nitrocellulose membrane using the I-blot apparatus (Invitrogen). Membranes were blocked with 0.2% I-Block–0.1%Tween solution (Tropix [Bedford, MA] or Sigma) and reacted with primary antibody followed by appropriate secondary antibody conjugated to horseradish peroxidase. Protein bands were visualized through enhanced chemiluminescence detection (GE Healthcare, Piscataway, NJ) with a G:Box imager (Syngene, Frederick, MD). Images were adjusted for total brightness and contrast with the Adobe Photoshop Elements 4.0 software. Band densitometry was calculated with the GeneTools software (Syngene).

TEM. Two separate sets of transmission electron microscopy (TEM) experiments were performed. In the first, MRC-5 cells grown to confluence in a T150 flask and infected with VZV vOka/Merck for 72 h were fixed with 2.5% glutaraldehyde for 5 min, removed with a scraper, and pelleted at 900 × *g* for 5 min. The cell pellet was stored at 4°C and shipped overnight to Electron Microscopy BioServices, LLC (Frederick, MD), for subsequent processing and imaging. Briefly, the pellet was washed in Millonig's sodium phosphate buffer, stored overnight at 4°C, postfixed in 1.0% osmium tetroxide, and washed with ultrapure water. Samples were stained with 2% aqueous uranyl acetate, dehydrated in a series of graded ethanol solutions, infiltrated, embedded in Spurr's plastic resin, polymerized overnight, and stored at −70°C. Ultrathin sections were cut, mounted onto mesh copper grids, and poststained with uranyl acetate and Reynold's lead citrate. Grids were then examined in a JEOL 1200 EX TEM at 60 kV.

In the second set of TEM experiments, MeWo cells were infected in culture dishes with VZV-32. At 96 h postinfection (hpi), the monolayer was prefixed for 20 min in 40% paraformaldehyde with 0.05% glutaraldehyde in 0.025 M cacodylate buffer (pH 7.2), washed well, postfixed for 1 h in 1% osmium tetroxide in s-collidine buffer, dehydrated, and embedded in epoxy resin. The samples were extracted from the tissue culture dish. Sections made with a diamond knife were stained with uranyl acetate and lead citrate and observed under a JEOL 1230 electron microscope, as described previously (4).

qRT-PCR. Infected cell monolayers were lysed with RLT-plus buffer (Qiagen USA, Valencia, CA). RNA was isolated using the RNeasy-Plus Mini Kit (Qiagen) per the manufacturer's recommended protocol. Eluates were processed with the Qiagen DNase Kit followed by Qiagen RNeasy MinElute Kit to ensure complete removal of DNA. RNA concentration and quality was determined by spectrophotometry. Multiplex quantitative reverse transcription-PCR (qRT-PCR) was performed starting with 125 ng total RNA on ABI 7900 instrument (Applied Biosystems, Foster City, CA) using the Quantitect multiplex RT-PCR kit (Qiagen) for the amplification of TATA-binding protein (TBP) and the indicated viral ORF. Relative levels of viral transcripts were determined using the conventional $\Delta\Delta CT$ method, normalizing to TBP transcript levels. Primer and probe sequences were as follows: TBP forward, 5′-GCCCGAAACGCCGAATAT-3′; TBP reverse, 5′-CGTGGCTCTCTTATCCTCATGA-3′; TBP probe, Hex-5′-ATCCCAAGCGGTTTGCTGCGG-3′-BHQ1; ORF14 forward, 5′-TTGGTTTACG

CGTCACCTTATAGA-3′; ORF14 reverse, 5′-CGGTAAATCTGGCATGCGTA T-3′, ORF14 probe, FAM-5′-CCGCACCGTCAACTGGGCAA-3′-BHQ1; ORF62 forward, 5′-CCGTATCGGGACTTCAACCA-3′; ORF62 reverse, 5′-GCATACGT AGTCGTCTTGTGTTAGC-3′; ORF62 probe, FAM-5′-ACCCAGAACGGAAG ATGTTGGCGA-BHQ1; ORF68 forward, 5′ CCCCAAGGCCAAAGACTCA-3′; ORF68 reverse, 5′-GAATCGGTGCGCGTAAAGTAA-3′; ORF68 probe, FAM-5′-TGAGGTGTCAGTGGAAGAAAATCACCCG-3′-BHQ1.

Immunofluorescence analysis. MRC-5 cells, grown and infected in eight-well slides, were fixed, permeabilized, and labeled with a rabbit anti-LC3 polyclonal antibody and with anti-VZV gE MAb clone 3B3. Alternatively, biopsies of human zoster vesicles and normal human skin were obtained previously as part of a characterization of VZV-specific proteins (49). The biopsies were sectioned and labeled with either a rabbit anti-LC3 polyclonal antibody, anti-VZV gC MAb clone 233, or rabbit anti-gC polyclonal antibody R19. In both sets of experiments the secondary antibodies were conjugated to Alexa Fluor fluorescent dyes. Draq5 was used to stain nuclei. Slides were viewed with a Zeiss 510 confocal microscope.

RESULTS

Autophagy is triggered in vOka/Merck-infected MRC-5 cells late in infection. The purpose of this set of experiments was to determine whether the autophagic pathway was induced in VZV infections. To this end, replicate cultures of MRC-5 cells were incubated with an inoculum consisting of trypsin-dispersed cells from a VZV vOka/Merck-infected monolayer exhibiting advanced CPE. The multiplicity of infection chosen was approximately 0.1 PFU per cell. At increasing intervals after infection, cells were harvested, solubilized, and subjected to immunoblotting with an antibody against LC3B. In order to track the progression of infection, antibodies against two VZV gene products, the abundantly expressed viral gE and the viral gC, were used; the latter was used as a marker of late stages of infection, inasmuch as its expression is delayed when VZV, including the vOka/Merck strain (data not shown), is grown in cultured cells.

As shown in Fig. 1, a band matching the M_r of LC3B-I (~16,000) was present in all lanes, as expected. A faster-migrating band, with apparent M_r of 14,000, corresponding to the expected M_r of the autophagosome-associated form LC3B-II (33), was occasionally detectable in lysates of mock-infected cells (Fig. 1, lanes 5 and 7). This baseline level is consistent with a basal level of autophagy being present and serving as a homeostatic mechanism in MRC-5 cells, as described in the introduction and in the literature (5). Importantly, LC3B-II accumulated starting at 48 hpi in a manner that overlapped with gC expression (Fig. 1, lanes 6 and 8). These data suggested that autophagy or programmed cell death type II was induced at late time points in VZV-infected cells. In order to assess the specificity of the autophagic response, we then reacted the lysates with an antibody against caspase 3, the major effector of apoptosis or programmed cell death type I. No significant induction of the apoptotic cascade was observed, as the cleaved, active fragment of caspase 3 was virtually undetectable under our experimental conditions. Upon densitometry analysis, the amounts of cleaved (active) caspase 3 at 72 hpi (Fig. 1, lane 8) ranged between 2% and 4% of the amount of full-length (inactive) procaspase 3. In order to provide a positive apoptotic control, we exposed MRC-5 cells to hyperosmotic medium containing 1 M sorbitol; the active form of caspase 3 was readily observed at only 4 h after exposure, and densitometry analysis indicated that its levels corresponded to 20% to 25% of the levels of procaspase 3 (data not shown).

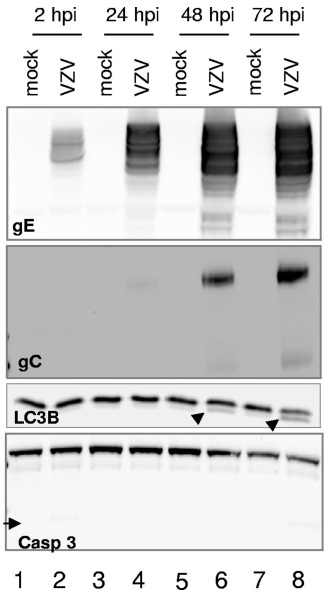

FIG. 1. Autophagy is triggered late in vOka/Merck infection of MRC-5 cells. Replicate cultures of MRC-5 cells were either mock infected or exposed to 0.1 PFU per cell of a virus inoculum consisting of trypsin-dispersed cells from a vOka/Merck-infected monolayer. At either 2, 24, 48, or 72 hpi, cells were harvested, solubilized, subjected to electrophoresis in a denaturing polyacrylamide gel, transferred to a nitrocellulose membrane, and reacted with antibodies against viral gE and gC and cellular proteins LC3B and caspase 3. The arrowheads point to LC3B-II, the PE-conjugated form of LC3B. The arrows point to caspase 3, the activation cleavage product of procaspase 3. Molecular weights: gE, ~88,000 to 98,000; gC, ~105,000; LC3B-I, ~16,000; LC3B-II, ~14,000; procaspase 3, ~35,000; active caspase 3, ~17,000.

Taken together, these data suggested that autophagy was induced at late stages of VZV infection of cultured cells.

Induction of autophagy in VZV-infected cultures results in cytoplasmic depletion and degradation of p62/SQSTM1. The purpose of this second set of experiments was to further investigate autophagy induction in VZV infection and specifically to determine whether the pathway could proceed to completion or whether it could be blocked at later stages by VZV-encoded functions. Replicate cultures of MRC-5 cells were infected using the same conditions described above, and at 72 hpi cells were fixed and examined by TEM. While the vast majority of cells in the monolayer were infected, due to the asynchronous nature of VZV infection the sample contained cells that had been infected for variable lengths of time. Thus, many cells exhibited capsids accumulating in the nucleus and had complete virions together with many L particles present on the cell surface (an example is shown in Fig. 2A). Other infected cells exhibited vacuolization similar to what had been reported previously (17), with large vacuoles enclosing virions, L particles, and some cellular material (Fig. 2B). Double-membrane autophagic compartments were frequently detected in these cells (an example is shown in Fig. 2B) and were occasionally found next to the vacuoles containing viral L particles and complete virions (Fig. 2B). Additionally, about 10 to 15% of cells exhibited the morphology of advanced autophagy, with extensive vacuolization and cytoplasmic depletion (Fig. 2C). Interestingly, the membranes of the vacuoles were some-

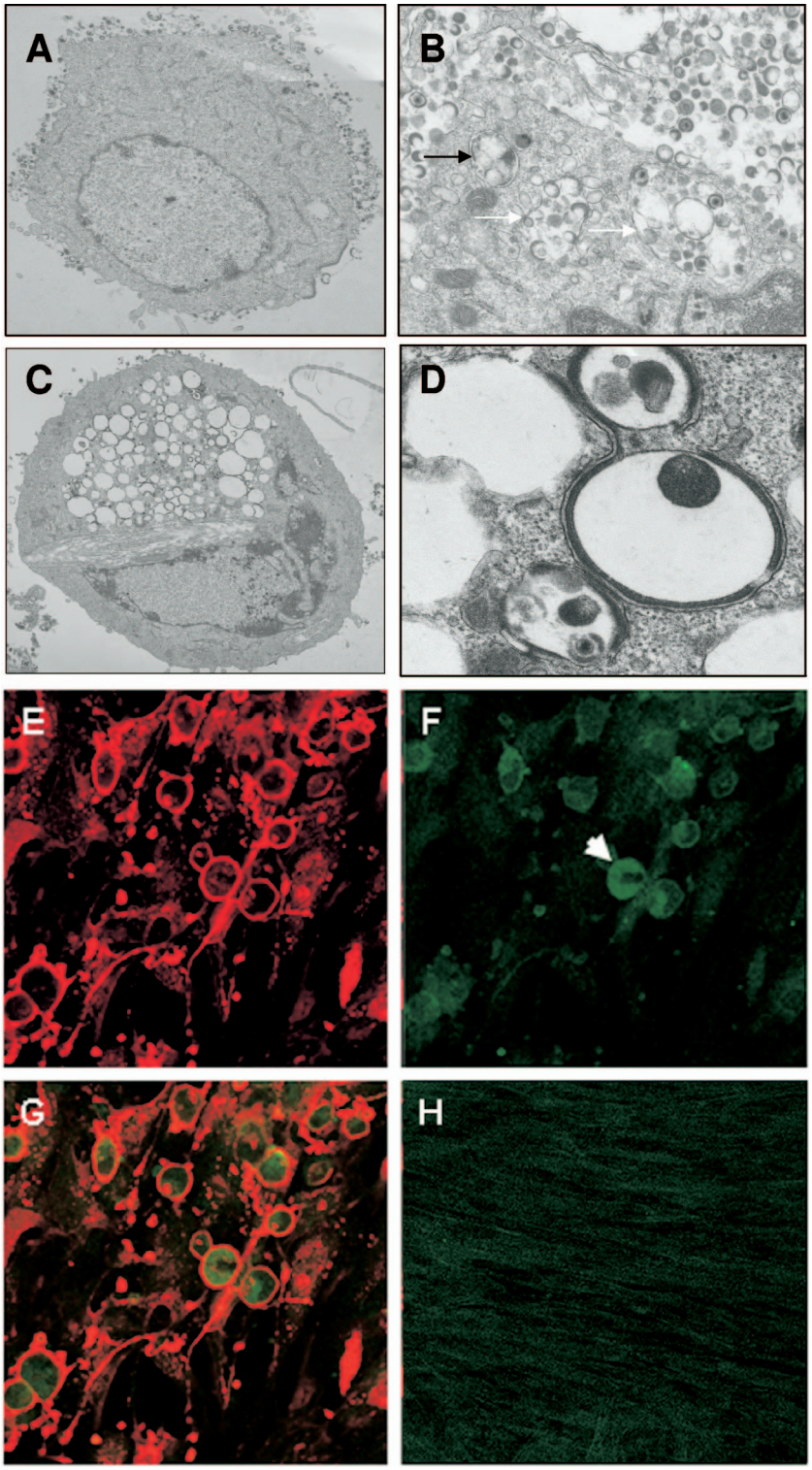

FIG. 2. Imaging of MRC-5 cells for demonstration of autophagy. (A to D) Electron micrographs of whole infected cells (A and C) or portions of the cytoplasm of infected cells (B and D). The black arrow in panel B points to an autophagic compartment; the white arrows in the same panel point to vacuolar structures containing complete virions, L particles, and additional material of cytoplasmic origin. (E to G) Immunofluorescence images of VZV-infected MRC-5 cells. Infected cell cultures were fixed and probed with antibodies against VZV gE (E) and LC3B (F) and then merged (G). The white arrow in panel F points to a representative cell positive for LC3B puncta. (H) Merged image of an uninfected cell culture stained with antibodies against VZV gE (red) and LC3B (green). The micrographs were acquired at the following magnifications: panel A, ×6,000; panel B, ×20,000; panel C, ×4,000; panel D, ×25,000; panels E to H, ×40.

times smooth and sometimes lined with electron-dense material (Fig. 2D). Also, it should be noted that we observed a smaller number of autophagic compartments in control, mock-infected cells, a result consistent with a basal level of autophagy being present in MRC-5 cells. As an additional control, infected cultures were subjected to immunofluorescence analysis with an antibody against LC3B. As described in the introduction, the staining pattern of LC3B-I, the cytosolic form of LC3B, is homogenous in the cytoplasm, while the PE-conjugated, autophagosome-associated form of LC3B-II stains in punctuate foci. A representative field is shown in Fig. 2E to H. Virtually every cell in the field stained strongly for viral gE (Fig. 2E), while the staining pattern of LC3B was heterogeneous: the majority of cells in the field showed faint diffuse staining, and a few individual cells showed intense punctuate staining, characteristic of the early stages of autophagy (Fig. 2F; Fig. 2G shows a merge of panels E and F). In contrast, little punctuate staining was visible in uninfected cells, consistent with a low basal level of autophagy (Fig. 2H). Upon enumeration of multiple fields, at least 15 to 20% of the cells exhibited some punctuate LC3B staining. It should be noted that an intrinsic limitation of these sets of experiments was that the samples contained cells at multiple stages of infection; therefore, it was not possible to quantify the number of autophagosome-positive cells or virus-induced autophagosomes per cell in a accurate manner by either electron microscopy or immunofluorescence techniques. However, when taken together, these data suggested that a subpopulation of cells in VZV-infected cultures was undergoing autophagy.

In order to confirm this observation, we investigated whether VZV infection affected the level of polyubiquitin-binding protein p62/SQSTM1 (sequestosome 1), a multifunctional protein that interacts with LC3B and is specifically degraded by the autophagic-lysosome pathway. Levels of p62/SQSTM1 are commonly measured to detect autophagic flux (22). To this end, replicate cultures of MRC-5 cells were infected with inoculum cells at a multiplicity of 0.1 PFU per cell. At 2, 17, 25, and 40 hpi, the medium was replaced with either fresh medium or medium containing 10 μM E64, a cell-permeative inhibitor of the lysosomal proteases cathepsins. The purpose of using E64 was to ascertain whether any changes in p62/SQSTM1 levels were due to autophagosome-lysosome degradation, as has been described elsewhere (3, 5). Cells were harvested and solubilized at 2 and 48 hpi and subjected to immunoblotting as described above, and band intensity was measured by densitometry analysis. As shown in Fig. 3, E64 treatment resulted in a slight increase in p62/SQSTM1 levels in mock-infected cells (compare lanes 3 and 5), again consistent with the occurrence of a homeostatic level of autophagy. Specifically, upon densitometry analysis, levels of p62/SQSTM1 in uninfected, E64-treated cells were 120% of those of uninfected, untreated cells. Infection with VZV resulted in a decrease of p62/SQSTM1 levels (Fig. 3, compare lane 4 to lane 3). Importantly, levels of p62/SQSTM1 were 153% higher in the lysates of infected cells exposed to E64 than in the lysates of infected untreated cells (Fig. 3, compare lanes 6 and 4). Such a phenotype is a common marker of ongoing autophagy (22). Therefore, these data indicated that in VZV-infected MRC-5 cells, the p62/SQSTM1 protein was degraded via the autophagic-lysosome pathway. Taken together, these results suggested that the VZV-induced autophagic pathway could proceed to completion and result in degradation of cytoplasmic proteins.

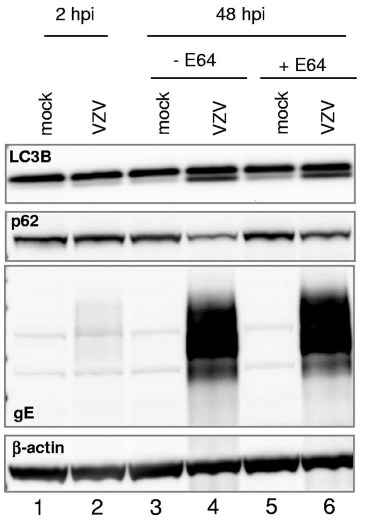

FIG. 3. Effect of the cathepsin inhibitor E64 on the levels of p62/SQSTM1 in MRC-5 cells infected with VZV vOka/Merck. Replicate cultures of MRC-5 cells were either mock infected or infected with VZV vOka/Merck as described in the legend to Fig. 1. After 2, 17, 25, and 40 h, the medium was replaced with either fresh medium alone or fresh medium containing 10 μM E64. At either 2 or 48 hpi, cells were harvested, solubilized, and subjected to immunoblotting with antibodies against VZV gE and cellular proteins p62/SQSTM1 and LC3B. β-Actin was used as a loading control. Molecular weights: p62/SQSTM1, ~62,000; β-actin, ~44,000.

Induction of autophagy in VZV-infected cells is not dependent on expression of VZV γ_2 gene products. The VZV gC is putatively considered a γ_2 gene product, based on HSV-1 gC data (36). Therefore, the temporal correlation between the accumulation of VZV gC protein and the appearance of autophagic markers raised the question whether a viral function encoded by a VZV true late gene constitutes an autophagic stimulus in infected cells. As an alternative hypothesis, autophagy might represent a cellular response to abundant accumulation of earlier gene products. Therefore, experiments were designed to discriminate between these two hypotheses by analyzing the accumulation of LC3B-II in the presence or absence of PAA, which inhibits the viral DNA polymerase and prevents expression of γ_2 gene products (20).

It is important to note that the VZV-induced activation of autophagy does not become significant before 48 hpi, which corresponds to more than one round of virus replication inasmuch as the VZV vOka/Merck strain can spread from cell to cell in a little over 16 h, similar to the case for VZV laboratory strains (38, 42). Therefore, in order to test our hypothesis, we could not initiate the PAA treatment at the time of infection and harvest at 48 hpi since, under such conditions, treatment would just prevent the multiple rounds of virus replication that are necessary to detect the autophagic phenotype (32). In fact, treatment with PAA starting at the time of infection prevented viral spread through the monolayer (data not shown). Rather, we initiated the treatment at a time postinfection corresponding, approximately, to one cycle of replication before the appearance of LC3B processing. Thus, we postulated that appropriate timing of the PAA exposure would result in a marked

reduction of gC accumulation while having a smaller or negligible effect on the accumulation of gene products belonging to the earlier kinetic classes.

In order to ensure that such a strategy was properly designed, we used RT-qPCR to compare expression of VZV ORF14 (encoding VZV gC), ORF62 (encoding the immediate early protein IE62), and ORF68 (encoding VZV gE) mRNAs in the presence or absence of PAA treatment. Briefly, MRC-5 cells were infected as described above and at 30 hpi were either mock treated or treated with PAA at a final concentration of 400 μg/ml. All cultures were harvested and lysed at 48 hpi, and total RNA was extracted and subjected to RT-qPCR. The PAA-induced inhibition of VZV ORFs was measured relative to control infections that had not been exposed to PAA. As expected, expression of the immediate-early gene ORF62 was not inhibited by PAA treatment (1.0% inhibition). In contrast, almost complete inhibition of ORF14 expression (90.2%) was achieved with the 18-h-long treatment. The transcription of ORF68 was also inhibited (16.7% inhibition), although less than the transcription of ORF14. In these experiments we saw no evidence that PAA altered the expression of cellular TBP, which was used as the endogenous reference transcript. These data indicated that PAA treatment was specific and effective.

We then tested whether PAA exposure, under these conditions, affected the accumulation of LC3B-II. Confluent cultures of MRC-5 cells were either mock infected or infected with VZV as described above. After 24 h, a replicate infection was harvested to provide a baseline control, and PAA treatment was initiated at either 24 or 30 hpi. Cultures were then harvested at 48 hpi, solubilized and subjected to immunoblotting with antibodies against VZV gE and gC and cellular LC3B. The results are shown in Fig. 4. As expected, at 24 hpi only a minimal amount of gC was detectable in the lysate (lane 2). At 48 hpi in the absence of treatment, gC was readily evident and an increase in the amount of LC3B-II, the faster-migrating form of LC3B, was apparent (lane 6). Accumulation of gE was not significantly affected by PAA treatment, consistent with the RNA data (compare lanes 6, 7, and 8). Treatment with PAA for either 18 or 24 h markedly decreased gC accumulation, as predicted for late gene products (compare the amounts of gC in lanes 7 and 8 to that in lane 6). On the other hand, the extent of LC3B-II accumulation was identical at 48 hpi regardless of PAA treatment (compare lanes 6, 7, and 8). Therefore, our results suggested that in VZV-infected cells, autophagy is triggered in temporal, but not causal, correlation with accumulation of PAA-sensitive viral gene products. Further, these results allowed us to formally assign VZV gC to the γ kinetic subclass.

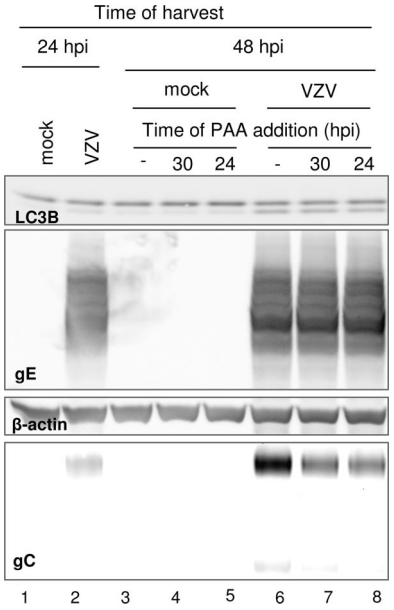

FIG. 4. Effect of PAA treatment on VZV vOka/Merck-infected MRC-5 cells. Replicate cultures of MRC-5 cells were either mock infected or infected with VZV vOka/Merck as described in the legend to Fig. 1. At 24 hpi, a set of replicate cultures was harvested to provide a baseline control. At either 24 or 30 hpi, cells were either mock treated or exposed to 400 μg/ml of PAA, and at 48 hpi, cells were harvested. All harvested cells were then solubilized, subjected to electrophoresis in a denaturing polyacrylamide gel, transferred to a nitrocellulose membrane, and reacted with antibodies against viral gE and gC and cellular proteins LC3B and β-actin.

VZV infection induces autophagy in MeWo cells. In the next series of experiments, we investigated whether autophagy was also induced by VZV in MeWo cells, which constitute a markedly different infection model than MRC-5 cells with regard to patterns of egress (17) and polykaryocyte formation and fusion; in particular, fusion is much more pronounced in MeWo cells, even when they are infected with the attenuated vOka/Merck strain (15). Two sets of experiments were thus performed. In the first set, replicate cultures of MeWo cells were infected with an inoculum consisting of trypsin-dispersed cells from a MeWo cell monolayer infected with the low-passage VZV-32 strain at a multiplicity of 1:8 (inoculum cells to uninfected cells). At increasing intervals after infection, cells were harvested, solubilized, and subjected to immunoblotting with antibodies against LC3B and gE. The results are shown in Fig. 5A. The relative amounts of LC3B-I and -II in mock-infected MeWo cells were different from those in mock-infected MRC-5 cells (compare the appearance of LC3B in Fig. 5A, lane 1, with that in lane 1 of Fig. 1). Such cell type-specific variability is common and not unanticipated (45). Furthermore, infection of MeWo cells proceeded with slower kinetics than that of MRC-5 cells under comparable conditions (data not shown). Importantly, as infection progressed over time, the amount of LC3B-II increased as expected (Fig. 5A, lanes 5 through 8).

In the second set of experiments, replicate cultures of MeWo cells were infected with VZV-32 as described above, and at 96 hpi cells were fixed and examined by TEM. As shown in Fig. 5B, compartments that displayed the features of early autophagosomes, inasmuch as they had double membranes and contained intact cytoplasmic material including melanin granules, were detectable in the cytoplasm of infected cells. Furthermore, Fig. 5C shows an MeWo cell polykaryocyte in which at least three nuclei were evident. Here, the cytoplasm in the syncytium was extensively vacuolar and depleted of material. Many vacuoles contained partially degraded, electron-dense material, characteristic of autophagic compartments. Interestingly, vacuoles with electron-dense linings comparable to those seen in Fig. 2 were not immediately apparent in this set of experiments. Finally, when MeWo cells infected with VZV-32 were exposed to E64, immunoblotting and densitom-

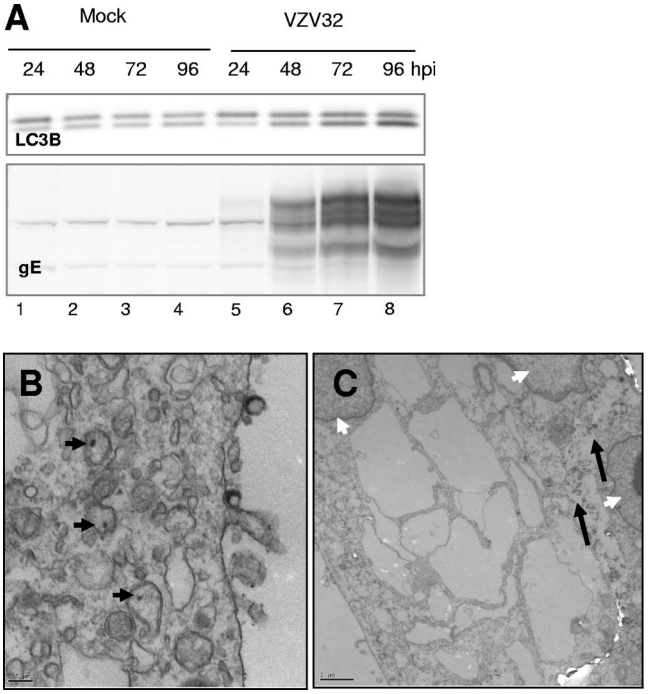

FIG. 5. VZV infection induces autophagy in MeWo cells. (A) Replicate cultures of MeWo cells were either mock infected or infected with a virus inoculum consisting of trypsin-dispersed cells from a VZV-32-infected MeWo cell monolayer exhibiting >70% CPE at a multiplicity of 1:8 (inoculum cells to target cells). At different time points after infection, cells were harvested, solubilized, and subjected to immunoblotting with antibodies against LC3B and viral gE. (B and C) Electron micrographs of MeWo cells infected with VZV-32 under the same conditions described for panel A, harvested at 96 hpi, and processed and imaged as described in Materials and Methods. Black arrowheads, early autophagosomes; white arrowheads, nuclei; black arrows, autophagic compartments. Bars, 0.2 μm (B) and 2 μm (C).

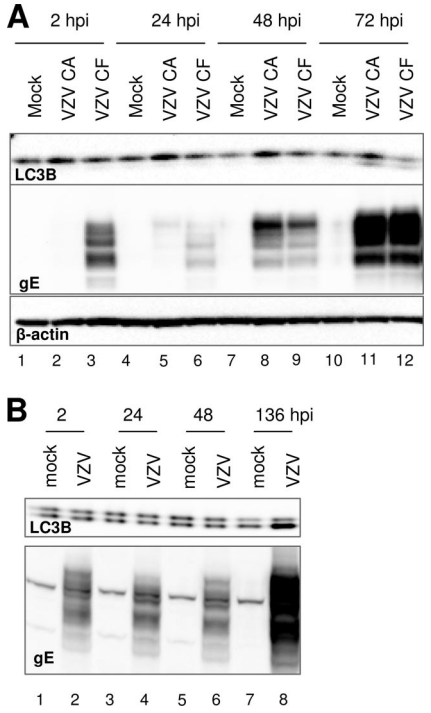

FIG. 6. Autophagy is induced in MRC-5 or MeWo cells infected with cell-free preparations of VZV vOka/Merck. (A) Replicate cultures of MRC-5 cells were mock infected or infected with inoculum consisting of either trypsin-dispersed (CA) or sonically disrupted (CF) infected MRC-5 cultures. Inoculum preparations had been titrated in advance, and the multiplicity of infection was approximately 0.02 PFU/cell. At different time points after infection, cells were harvested, solubilized, and subjected to immunoblotting with antibodies against β-actin, LC3B, and viral gE. (B) Replicate cultures of MeWo cells were either mock infected or infected with a virus inoculum consisting of cell-free VZV vOka/Merck at a multiplicity of infection of approximately 0.01 PFU/cell. At various time points after infection, cells were harvested, solubilized, and subjected to immunoblotting with antibodies against LC3B and viral gE.

etry analysis showed that the amount of p62/SQSTM1 increased with a pattern comparable to that observed in the experiments reported in Fig. 3 (data not shown).

Infection of either MRC-5 or MeWo cells with cell-free preparations of VZV induces LC3B processing. The experiments presented above indicated that induction of autophagy occurred when either MRC-5 or MeWo cells were infected with inoculum consisting of trypsin-dispersed infected cells. We then tested whether the same phenotype was apparent when cells were infected with sonically disrupted infected cells, i.e., a "cell-free" virus preparation. It should be noted that, due to the very low yields of infectious VZV, as described in the introduction, the highest multiplicity of infection attainable with this method was about 0.02 PFU/cell. For the same reason, such inoculum preparations also contained large amounts of input material compared to an inoculum consisting of trypsin-dispersed cells. In the first experiment, replicate cultures of MRC-5 cells were infected either with trypsin-dispersed infected MRC-5 cells or with a cell-free preparation of VZV vOka/Merck at a multiplicity of approximately 0.02 PFU/cell, thus providing a direct comparison of the two modalities of infection.

At increasing intervals after infection, cells were harvested and the lysates were immunoblotted with antibodies against LC3B and gE. The results are shown in Fig. 6A. Because of the low yield of cell-free infectious VZV, more input gE was present in the cell-free inoculum than in the inoculum consisting of infected cells, (compare lanes 2 and 3). In addition, the infection from the cell-free preparation progressed at a low rate, so that virtually no newly synthesized gE was detectable up to 48 hpi (lane 9); gE levels present at 24 hpi (lane 6) represented remnants of the original inoculum material. Importantly, by 72 hpi the processed form of LC3B was detectable in the lysates of cells infected with either trypsinized cells or sonically disrupted cell lysates.

In the second series of experiments, replicate cultures of MeWo cells were infected with a cell-free preparation of VZV vOka/Merck at a multiplicity of approximately 0.01 PFU per cell. As shown in Fig. 6B, infection under these conditions proceeded very slowly. This observation was not surprising given our infection conditions, in which we used a low multiplicity of infection and combined both the cell substrate and inoculum type in which the spread of VZV is the slowest. Nonetheless, at 136 hpi, a marked accumulation of LC3B-II was observed (compare lanes 7 and 8). We concluded from these data that infection with either low-passage laboratory

VZV or attenuated VZV induced autophagy at late time points in both fibroblast and melanoma cells, regardless of whether the viral inoculum consisted of live infected cells or cell-free virus preparations.

Analysis of autophagosomes in human zoster vesicles. The experiments with VZV-infected cultured cells described above suggested that autophagy may play a role in VZV pathogenesis. Since no prior studies have investigated this hypothesis, we compared the subcellular appearance of LC3B in biopsies of normal human skin and zoster vesicles. In an earlier report (49) we demonstrated that gE and gH were easily detected in vesicles. Recently, we documented that VZV gC was also expressed abundantly in skin vesicles, in contrast to the case for cultured cells (41). Skin vesicles were sectioned and labeled with a primary antibody against LC3B, followed by incubation with a fluorochrome-conjugated secondary antibody. Cells with numerous characteristic LC3B-positive puncta were easily distinguished within the vesicle tissue at low magnification (Fig. 7A). The punctuate pattern of LC3B staining appeared within single cells and small clusters of cells interspersed throughout the vesicle (Fig. 7B). To more precisely assess the distribution of the autophagosomes, we obtained a Z-stack of images at a magnification of ×100. Figure 7C and D show images 7 and 11, respectively, from a Z-stack of 20 images with a combined thickness of 13.5 μm. These images indicate that the LC3B-II puncta were distributed throughout the cytoplasm of the vesicle cells, matching the intracellular localization of autophagosomes (22). When adjacent sections of the same vesicle were immunostained with antibodies against VZV gC plus a nuclear stain, all cells in the vesicle were positive (Fig. 7E). As another control, normal skin tissues were similarly incubated with LC3B antibody, but only a faint background was detected (Fig. 7F). Note that the vesicle in Fig. 7B and the normal skin in Fig. 7E are shown at the same magnification. Another section of the vesicle was routinely stained with hematoxylin and eosin as an additional control (data not shown). We note that no biopsy samples were available from vesicles at early stages, so we could not assess the progression of autophagy from the early to the late stages of human vesicle formation.

DISCUSSION

The experiments presented in this paper were initiated to enhance our understanding of the interplay between VZV and the host cell, with particular focus on the late stages of infection. The most important finding of this report is that in VZV-infected cells we observed an accumulation of the autophagosome-associated form of LC3B, a marker of induction of autophagy. The modification of LC3B correlated with increased formation of autophagosomes, with cytoplasmic depletion, and with degradation of the autophagy marker p62/SQSTM1 polyubiquitin-binding protein.

We also investigated whether apoptosis was present in our cultures, since the autophagic and apoptotic pathways can affect each other and because various reports have shown that apoptosis can be induced by VZV infection, in a cell type- and possibly virus strain-dependent manner (11, 19). We report that we did not detect major signs of apoptosis in MRC-5 cells at up to 72 hpi with the vOka/Merck strain. Although it is likely that a longer incubation time would lead to more extensive caspase 3 activation and other apoptotic phenotypes, more studies will be needed to characterize the kinetics of apoptosis induction in MRC-5 cells infected with parental versus vaccine VZV Oka strains. Within the scope of these studies, the data showed that autophagy was induced on its own, well in advance of any signs of apoptosis.

Further, autophagy appeared to be a common outcome of VZV infection in cell cultures, since it was detected independently of the multiplicity of infection chosen, of the VZV strain used (attenuated or wild type), of the type of virus inoculum used (cell associated or cell free), and of the cell substrate (fibroblast or epithelial). While induction of autophagy in cultured cells appeared concomitantly with accumulation of the viral late gene product gC, we demonstrated that the two phenotypes were not causally related, since exposure to PAA, an inhibitor of viral DNA replication, decreased gC expression but did not affect induction of autophagy. Finally, we report that autophagosomes were detectable in biopsies of human zoster vesicles but not in biopsies of normal skin. Therefore, we propose that VZV infection induces the autophagic pathway in both cultured cells and human skin, that autophagy results in degradation of the p62/SQSTM1 polyubiquitin-binding protein and extensive depletion of cytoplasmic material, and that autophagy appears to be triggered by a function encoded by a VZV gene product that is not prevented by treatment with PAA.

Many aspects of the VZV-mediated induction of autophagy that we have reported here will need to be addressed with further experimentation. In particular, the mechanism responsible for induction of autophagy in VZV infection remains to be identified.

Furthermore, it will be very interesting to investigate whether the yields of infectious VZV particles in cultured cells are negatively affected by activation of the autophagic pathway. VZV particles are known to accumulate in cytoplasmic vacuoles, where it has been proposed that they are degraded by acid hydrolases (13). A role for MPR^{ci} was suggested in this process, since cells deficient in MPR^{ci} constitutively secreted both lysosomal enzymes and VZV particles (6). The data presented here show that VZV virions accumulated together with L particles in vacuoles alongside autophagosomes. Importantly, we showed that the VZV-induced degradation of the autophagic marker p62/SQSTM1 is inhibited by treatment with E64, an inhibitor of cathepsins, a family of lysosomal hydrolases. Whether the autophagosomal machinery is involved in vacuolar accumulation and possibly in degradation of VZV virions and L particles or whether the latter phenotype is the result of a distinct signaling pathway will have to be ascertained.

Many but not all vacuoles present in MRC-5 cells infected with the vaccine strain exhibited an electron-dense lining that was reminiscent of trans-Golgi network-derived cisternae observed previously in fibroblasts infected with a gI^- VZV mutant (48). However, the vOka/Merck attenuated strain does not contain mutations in ORF67, which encodes gI. Furthermore, ORF67 mRNA was expressed throughout infection (data not shown), and infected cells readily stained for gI in immunofluorescence experiments (data not shown). Therefore, the densely lined vacuoles did not appear to be related to either the absence of gI or the attenuation of the vOka/Merck vaccine strain.

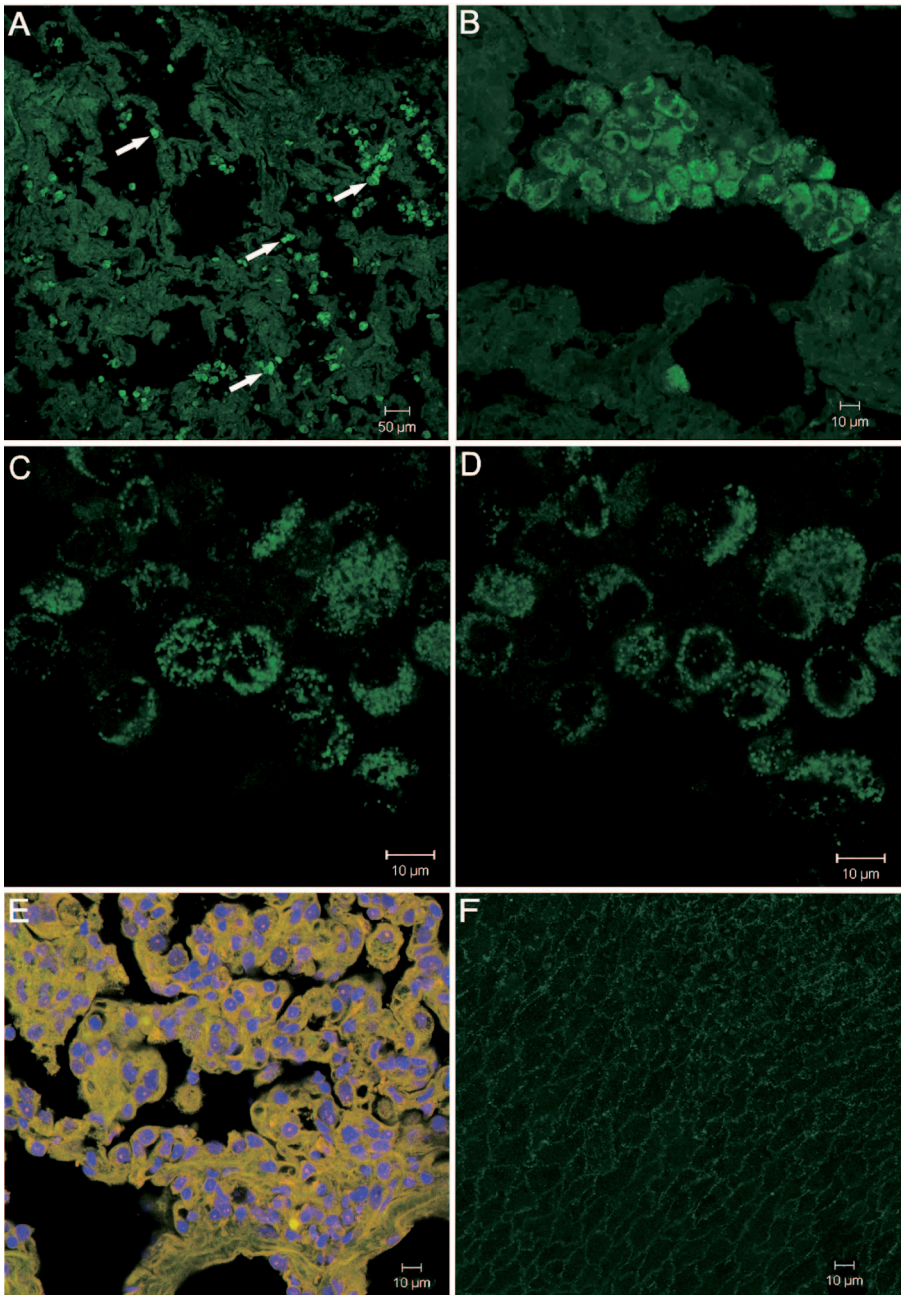

FIG. 7. Detection of autophagosomes in a skin biopsy from a human zoster vesicle. (A to D) A human zoster skin vesicle was sectioned and labeled with rabbit anti-LC3B polyclonal antibody, followed by incubation with a goat anti-rabbit secondary antibody conjugated to a 488 fluorophore. Images were collected on a Zeiss confocal microscope at a magnification of ×10 (A), ×40 (B), or ×100 (C and D). The white arrows in panel A indicate four examples of cells showing punctuate LC3B staining. Panels C and D are images 7 and 11, respectively, from a Z-stack of 20 images with a combined thickness of 13.5 μm. (E) Zoster vesicle section labeled with anti-VZV gC MAb (green), rabbit anti-gC polyclonal antibody (red), and the nuclear stain Draq5 (blue). Magnification, ×40. (F) Section of uninfected human skin labeled with rabbit anti-LC3B polyclonal antibody (green). Magnification, ×40.

Finally, the association of autophagy with VZV pathogenesis was an important extension of our investigations. During primary VZV infection (chicken pox), the virus spreads to the skin after a viremia, while after reactivation (herpes zoster), the virus travels via a neuronal route from the dorsal root ganglia. In both chicken pox and zoster, skin vesicles are the final site of VZV replication and virus formation. While the architecture of skin vesicles immunostained with a variety of anti-VZV antibodies has been previously delineated (41, 49), the fact the zoster vesicles contain autophagosomes is an intriguing finding. The punctuate LC3B-positive autophagosomes were easily detected by confocal microscopy throughout the skin vesicles. In future investigations, it will be informative to determine whether the percentage of cells with autophago-

somes changes during progression from early to late stages of vesicle formation or whether autophagy is differentially induced in high-risk groups, e.g., the elderly, who develop more severe zoster.

Our findings highlight a novel and potentially important difference in the properties of VZV compared to those of the related alphaherpesvirus HSV-1. Interestingly, HSV-1 replication induces autophagy, but the HSV-1 neurovirulence factor ICP34.5, the product of the $\gamma_1$34.5 gene, can block it by interacting with the cellular autophagy regulator Beclin1 (2, 34). Suppression of autophagy has marginal effects on the replication of HSV-1 in cultured cells but is a major determinant of HSV-1 neurovirulence in animal models (2, 34). Importantly, the HSV-1 $\gamma_1$34.5 gene has no VZV ortholog (14, 37), and thus our results are consistent with a model in which VZV does not evade the host autophagy machinery in vitro or in vivo. Our findings advance the understanding of the complex virus-host interactions that occur during VZV infection.

ACKNOWLEDGMENTS

The studies presented here were fully supported by Merck & Co., Inc. Charles Grose is the recipient of funding from Merck & Co.

We thank John Bernbaum of Electron Microscopy BioServices, LLC, for assistance with electron microscopy experiments and John Aunins and Katey Owen for invaluable discussions and critical reading of the manuscript.

REFERENCES

1. **Ait-Goughoulte, M., T. Kanda, K. Meyer, J. S. Ryerse, R. B. Ray, and R. Ray.** 2008. Hepatitis C virus genotype 1a growth and induction of autophagy. J. Virol. **82:**2241–2249.
2. **Alexander, D. E., S. L. Ward, N. Mizushima, B. Levine, and D. A. Leib.** 2007. Analysis of the role of autophagy in replication of herpes simplex virus in cell culture. J. Virol. **81:**12128–12134.
3. **Bjorkoy, G., T. Lamark, A. Brech, H. Outzen, M. Perander, A. Overvatn, H. Stenmark, and T. Johansen.** 2005. p62/SQSTM1 forms protein aggregates degraded by autophagy and has a protective effect on huntingtin-induced cell death. J. Cell Biol. **171:**603–614.
4. **Carpenter, J. E., J. A. Hutchinson, W. Jackson, and C. Grose.** 2008. Egress of light particles among filopodia on the surface of varicella-zoster virus-infected cells. J. Virol. **82:**2821–2835.
5. **Chaumorcel, M., S. Souquere, G. Pierron, P. Codogno, and A. Esclatine.** 2008. Human cytomegalovirus controls a new autophagy-dependent cellular antiviral defense mechanism. Autophagy **4:**46–53.
6. **Chen, J. J., Z. Zhu, A. A. Gershon, and M. D. Gershon.** 2004. Mannose 6-phosphate receptor dependence of varicella zoster virus infection in vitro and in the epidermis during varicella and zoster. Cell **119:**915–926.
7. **Cohen, J. E., S. E. Straus, and A. M. Arvin.** 2007. Varicella-zoster virus replication, pathogenesis and management, p. 2773–2818. *In* B. N. Fields, D. M. Knipe, P. M. Howley, D. E. Griffin, R. A. Lamb, M. A. Martin, B. Roizman, and S. E. Straus (ed.), Fields virology. Lippincott-Raven, Philadelphia, PA.
8. **Cuervo, A. M.** 2004. Autophagy: in sickness and in health. Trends Cell Biol. **14:**70–77.
9. Reference deleted.
10. Reference deleted.
11. **Erazo, A., M. B. Yee, N. Osterrieder, and P. R. Kinchington.** 2008. Varicella-zoster virus open reading frame 66 protein kinase is required for efficient viral growth in primary human corneal stromal fibroblast cells. J. Virol. **82:**7653–7665.
12. **Espert, L., P. Codogno, and M. Biard-Piechaczyk.** 2007. Involvement of autophagy in viral infections: antiviral function and subversion by viruses. J. Mol. Med. **85:**811–823.
13. **Gershon, A. A., D. L. Sherman, Z. Zhu, C. A. Gabel, R. T. Ambron, and M. D. Gershon.** 1994. Intracellular transport of newly synthesized varicella-zoster virus: final envelopment in the trans-Golgi network. J. Virol. **68:**6372–6390.
14. **Gomi, Y., H. Sunamachi, Y. Mori, K. Nagaike, M. Takahashi, and K. Yamanishi.** 2002. Comparison of the complete DNA sequences of the Oka varicella vaccine and its parental virus. J. Virol. **76:**11447–11459.
15. **Grose, C.** 1996. Pathogenesis of infection with varicella vaccine. Infect. Dis. Clin. N. Am. **10:**489–505.
16. **Grose, C.** 2005. Varicella vaccination of children in the United States: assessment after the first decade 1995–2005. J. Clin. Virol. **33:**89–98.
17. **Harson, R., and C. Grose.** 1995. Egress of varicella-zoster virus from the melanoma cell: a tropism for the melanocyte. J. Virol. **69:**4994–5010.
18. **Hayakawa, Y., S. Torigoe, K. Shiraki, K. Yamanishi, and M. Takahashi.** 1984. Biologic and biophysical markers of a live varicella vaccine strain (Oka): identification of clinical isolates from vaccine recipients. J. Infect. Dis. **149:**956–963.
19. **Hood, C., A. L. Cunningham, B. Slobedman, R. A. Boadle, and A. Abendroth.** 2003. Varicella-zoster virus-infected human sensory neurons are resistant to apoptosis, yet human foreskin fibroblasts are susceptible: evidence for a cell-type-specific apoptotic response. J. Virol. **77:**12852–12864.
20. **Jones, P. C., and B. Roizman.** 1979. Regulation of herpesvirus macromolecular synthesis. VIII. The transcription program consists of three phases during which both extent of transcription and accumulation of RNA in the cytoplasm are regulated. J. Virol. **31:**299–314.
21. **Kabeya, Y., N. Mizushima, T. Ueno, A. Yamamoto, T. Kirisako, T. Noda, E. Kominami, Y. Ohsumi, and T. Yoshimori.** 2000. LC3, a mammalian homologue of yeast Apg8p, is localized in autophagosome membranes after processing. EMBO J. **19:**5720–5728.
22. **Klionsky, D. J., H. Abeliovich, P. Agostinis, D. K. Agrawal, G. Aliev, D. S. Askew, M. Baba, E. H. Baehrecke, B. A. Bahr, A. Ballabio, B. A. Bamber, D. C. Bassham, E. Bergamini, X. Bi, M. Biard-Piechaczyk, J. S. Blum, D. E. Bredesen, J. L. Brodsky, J. H. Brumell, U. T. Brunk, W. Bursch, N. Camougrand, E. Cebollero, F. Cecconi, Y. Chen, L. S. Chin, A. Choi, C. T. Chu, J. Chung, P. G. Clarke, R. S. Clark, S. G. Clarke, C. Clave, J. L. Cleveland, P. Codogno, M. I. Colombo, A. Coto-Montes, J. M. Cregg, A. M. Cuervo, J. Debnath, F. Demarchi, P. B. Dennis, P. A. Dennis, V. Deretic, R. J. Devenish, F. Di Sano, J. F. Dice, M. Difiglia, S. Dinesh-Kumar, C. W. Distelhorst, M. Djavaheri-Mergny, F. C. Dorsey, W. Droge, M. Dron, W. A. Dunn, Jr., M. Duszenko, N. T. Eissa, Z. Elazar, A. Esclatine, E. L. Eskelinen, L. Fesus, K. D. Finley, J. M. Fuentes, J. Fueyo, K. Fujisaki, B. Galliot, F. B. Gao, D. A. Gewirtz, S. B. Gibson, A. Gohla, A. L. Goldberg, R. Gonzalez, C. Gonzalez-Estevez, S. Gorski, R. A. Gottlieb, D. Haussinger, Y. W. He, K. Heidenreich, J. A. Hill, M. Hoyer-Hansen, X. Hu, W. P. Huang, A. Iwasaki, M. Jaattela, W. T. Jackson, X. Jiang, S. Jin, T. Johansen, J. U. Jung, M. Kadowaki, C. Kang, A. Kelekar, D. H. Kessel, J. A. Kiel, H. P. Kim, A. Kimchi, T. J. Kinsella, K. Kiselyov, K. Kitamoto, E. Knecht, et al.** 2008. Guidelines for the use and interpretation of assays for monitoring autophagy in higher eukaryotes. Autophagy **4:**151–175.
23. **Klionsky, D. J., J. M. Cregg, W. A. Dunn, Jr., S. D. Emr, Y. Sakai, I. V. Sandoval, A. Sibirny, S. Subramani, M. Thumm, M. Veenhuis, and Y. Ohsumi.** 2003. A unified nomenclature for yeast autophagy-related genes. Dev. Cell **5:**539–545.
24. **Komatsu, M., S. Waguri, M. Koike, Y. S. Sou, T. Ueno, T. Hara, N. Mizushima, J. Iwata, J. Ezaki, S. Murata, J. Hamazaki, Y. Nishito, S. Iemura, T. Natsume, T. Yanagawa, J. Uwayama, E. Warabi, H. Yoshida, T. Ishii, A. Kobayashi, M. Yamamoto, Z. Yue, Y. Uchiyama, E. Kominami, and K. Tanaka.** 2007. Homeostatic levels of p62 control cytoplasmic inclusion body formation in autophagy-deficient mice. Cell **131:**1149–1163.
25. Reference deleted.
26. **Ku, B., J. S. Woo, C. Liang, K. H. Lee, H. S. Hong, X. E., K. S. Kim, J. U. Jung, and B. H. Oh.** 2008. Structural and biochemical bases for the inhibition of autophagy and apoptosis by viral BCL-2 of murine gamma-herpesvirus 68. PLoS Pathog. **4:**e25.
27. **Lee, D. Y., and B. Sugden.** 2008. The latent membrane protein 1 oncogene modifies B-cell physiology by regulating autophagy. Oncogene **27:**2833–2842.
28. **Levine, B.** 2005. Eating oneself and uninvited guests: autophagy-related pathways in cellular defense. Cell **120:**159–162.
29. **Liang, X. H., L. K. Kleeman, H. H. Jiang, G. Gordon, J. E. Goldman, G. Berry, B. Herman, and B. Levine.** 1998. Protection against fatal Sindbis virus encephalitis by beclin, a novel Bcl-2-interacting protein. J. Virol. **72:**8586–8596.
30. **Liu, Y., M. Schiff, K. Czymmek, Z. Talloczy, B. Levine, and S. P. Dinesh-Kumar.** 2005. Autophagy regulates programmed cell death during the plant innate immune response. Cell **121:**567–577.
31. Reference deleted.
32. **May, D. C., M. R. Miller, and F. Rapp.** 1977. The effect of phosphonoacetic acid on the in vitro replication of varicella-zoster virus. Intervirology **8:**83–91.
33. **Mizushima, N., and T. Yoshimori.** 2007. How to interpret LC3 immunoblotting. Autophagy **3:**542–545.
34. **Orvedahl, A., D. Alexander, Z. Talloczy, Q. Sun, Y. Wei, W. Zhang, D. Burns, D. A. Leib, and B. Levine.** 2007. HSV-1 ICP34.5 confers neurovirulence by targeting the Beclin 1 autophagy protein. Cell Host Microbe **1:**23–35.
35. **Pattingre, S., A. Tassa, X. Qu, R. Garuti, X. H. Liang, N. Mizushima, M. Packer, M. D. Schneider, and B. Levine.** 2005. Bcl-2 antiapoptotic proteins inhibit Beclin 1-dependent autophagy. Cell **122:**927–939.
36. **Peake, M. L., P. Nystrom, and L. I. Pizer.** 1982. Herpesvirus glycoprotein synthesis and insertion into plasma membranes. J. Virol. **42:**678–690.
37. **Peters, G. A., S. D. Tyler, C. Grose, A. Severini, M. J. Gray, C. Upton, and G. A. Tipples.** 2006. A full-genome phylogenetic analysis of varicella-zoster virus reveals a novel origin of replication-based genotyping scheme and

evidence of recombination between major circulating clades. J. Virol. **80:** 9850–9860.
38. **Rapp, F., and D. Vanderslice.** 1964. Spread of zoster virus in human embryonic lung cells and the inhibitory effect of lododeoxyuridine. Virology **22:** 321–330.
39. **Reggiori, F., and D. J. Klionsky.** 2002. Autophagy in the eukaryotic cell. Eukaryot. Cell **1:**11–21.
40. **Shintani, T., and D. J. Klionsky.** 2004. Autophagy in health and disease: a double-edged sword. Science **306:**990–995.
41. **Storlie, J., J. E. Carpenter, W. Jackson, and C. Grose.** 2008. Discordant varicella-zoster virus glycoprotein C expression and localization between cultured cells and human skin vesicles. Virology **382:**171–181.
42. **Storlie, J., W. Jackson, J. Hutchinson, and C. Grose.** 2006. Delayed biosynthesis of varicella-zoster virus glycoprotein C: upregulation by hexamethylene bisacetamide and retinoic acid treatment of infected cells. J. Virol. **80:**9544–9556.
43. **Takahashi, M.** 1986. Clinical overview of varicella vaccine: development and early studies. Pediatrics **78:**736–741.
44. **Takahashi, M.** 1984. Development and characterization of a live varicella vaccine (Oka strain). Biken J. **27:**31–36.
45. **Tanida, I., N. Minematsu-Ikeguchi, T. Ueno, and E. Kominami.** 2005. Lysosomal turnover, but not a cellular level, of endogenous LC3 is a marker for autophagy. Autophagy **1:**84–91.
46. **Tanida, I., T. Ueno, and E. Kominami.** 2004. LC3 conjugation system in mammalian autophagy. Int. J. Biochem. Cell Biol. **36:**2503–2518.
47. **Tillieux, S. L., W. S. Halsey, E. S. Thomas, J. J. Voycik, G. M. Sathe, and V. Vassilev.** 2008. Complete DNA sequences of two Oka strain varicella-zoster virus genomes. J. Virol. **82:**11023–11044.
48. **Wang, Z. H., M. D. Gershon, O. Lungu, Z. Zhu, S. Mallory, A. M. Arvin, and A. A. Gershon.** 2001. Essential role played by the C-terminal domain of glycoprotein I in envelopment of varicella-zoster virus in the trans-Golgi network: interactions of glycoproteins with tegument. J. Virol. **75:**323–340.
49. **Weigle, K. A., and C. Grose.** 1983. Common expression of varicella-zoster viral glycoprotein antigens in vitro and in chickenpox and zoster vesicles. J. Infect. Dis. **148:**630–638.